International Journal of Thermofluids 22 (2024) 100619

Contents lists available at ScienceDirect

International Journal of Thermofluids

journal homepage: www.sciencedirect.com/journal/international-journal-of-thermofluids

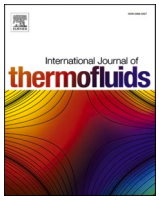

Viscous dissipation effects on slip flow heat transfer in rhombic microchannels

Pamela Vocale [a,*], Gian Luca Morini [b]

[a] Department of Engineering and Architecture, University of Parma, Parma, Italy
[b] DIN – Alma Mater Studiorum Università di Bologna, Viale Risorgimento 3, 40135 Bologna, Italy

ARTICLE INFO

Keywords:
Micro flow
Rarefaction effects
Viscous dissipation
Noncircular cross-sections

ABSTRACT

This study aimed to numerically investigate the viscous dissipation effect on forced convection in rhombic microchannels for gases in a slip flow regime. The numerical analysis was carried out by assuming a 2D steady-state flow. The solution of governing equations was obtained by adopting the finite element method and assuming that the fluid is Newtonian, with constant thermophysical properties, and in a fully developed laminar flow regime. The solution of the momentum equation is obtained by considering a first-order boundary condition, while the solution of the energy balance equation is obtained by assuming a constant wall heat flux (H2 boundary condition) and taking into account the wall temperature jump. The validation of the numerical model was carried out using the data available in the scientific literature. The numerical outcomes obtained for several values of the acute angle of the rhombus, the Knudsen number (i.e., rarefaction effects), and the Brinkman number (i.e., viscous dissipation effects) reveal that viscous forces play an opposite role with respect to rarefaction and significantly affect the convective heat transfer coefficient, especially for low Knudsen numbers and for high values of the acute angle. In particular, it was observed that Nu is significantly affected by the Brinkman number for acute angles higher than 50°.

Introduction

The dynamics of fluids and their interaction with solid surfaces in microsystems are very different from those in large systems. When the characteristic length of the system becomes very small, the effects (e.g., thermal creep, rarefaction, compressibility, viscous heating) that in macrosystems can be considered negligible may be important.

In particular, when the gases through the microchannel are characterized by pressure below the atmospheric value (e.g., in vacuum technology and gas chromatography), the continuum hypothesis is no longer valid because of a layering phenomenon in the near-wall region [1].

Moreover, the viscous heating effects may be very significant, even for low-viscosity fluids or low-velocity flows, when the characteristic length of the system becomes very small and/or the temperature difference is very small.

The impact of rarefaction and viscous dissipation has been investigated in microchannels with circular, rectangular, trapezoidal and elliptical cross-sections [2–10]. In particular, Tunc and Bayazitoglu studied the impact of viscous dissipation in circular microchannels by finding that for Brinkman number equal to 0.01 the Nusselt number could reduce up to 8 %. van Rij et al. [8], who investigated the effect of viscous heating on convective heat transfer in rectangular microchannels in the slip regime, found that for a Brinkman number equal to 0.05, the Nusselt number could reduce up to 24 %. Kuddusi [9], who carried out the analysis of slip flow heat transfer in trapezoidal microchannels, including the impact of viscous dissipation, observed that for Brinkman number equal to 0.005, the maximum decrease in the Nusselt number was 2 %. A higher reduction in the Nusselt number was found by Vocale et al. [10], who presented a numerical analysis of the impact of rarefaction and viscous dissipation effects in elliptical microchannels. They concluded that the Nusselt number could be overestimated by up to 59 % by neglecting the effects of viscous heating.

Moreover, many researchers have investigated heat transfer and fluid flow in microchannels characterized by noncircular cross-sections by presenting approximate or analytical solutions for simple geometries [13–17].

Recently, Mukherjee et al. [18] analyzed the influence of viscous heating on the performance of microchannels featuring circular, semi-circular, triangular, rectangular, and square cross-sections by considering power-law fluids. They found that for the Brinkman number

* Corresponding author.
E-mail address: pamela.vocale@unipr.it (P. Vocale).

https://doi.org/10.1016/j.ijft.2024.100619

Available online 1 March 2024

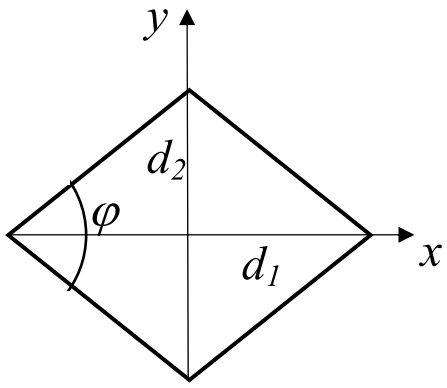

Fig. 1. Investigated geometry.

equal to 0.1, the maximum reduction in the Nusselt number was about 19 %.

More recently, Loh et al. [19] studied the impact of viscous dissipation on the convective heat transfer coefficient in nanofluids flowing in parallel-plate microchannels. The maximum rate of change in the Nusselt number was about 17 %.

However, other geometries need attention because of improvements in the microfabrication technique or the combination of simple geometries. Among these, rhombic microchannels can be found. They can be fabricated using a novel process [11], or can be obtained from triangular microchannels or from the etching of rectangular microchannels [12].

Shams et al. [20] investigated the performance of rhombic microchannels. The numerical outcomes revealed that the Nusselt numbers were considerably influenced by the aspect ratio and the Knudsen number.

Saha et al. [12] recently numerically investigated laminar water flows in rhombic microchannels by considering two different thermal boundary conditions. Their numerical outcomes highlighted that the influence of the acute angle on the convective heat transfer coefficient is significant for acute angles greater than 10°.

More recently, Vocale and Morini [21] numerically investigated the influence of rarefaction in rhombic microchannels. Their findings revealed that both the rarefaction degree and the acute angle strongly affected the heat transfer mechanism.

From the literature review, it is evident that further investigations are needed to properly characterize the performance of rhombic microchannels. In particular, the analysis carried out in other cross-section geometries highlighted that another effect that may significantly affect the thermal performance of microchannels is viscous heating. Therefore, this paper deepened the knowledge of scaling effects by presenting a numerical investigation of the influence of rarefaction and viscous dissipation in microchannels with rhombic cross-sections. The fully developed forced convection problem for Newtonian fluid with constant properties was investigated under uniform wall heat flux boundary conditions. The numerical analysis was carried out by considering the slip flow regime because most of the microsystems that use gases as working fluids, such as microvalves and micropumps, work within the slip flow regime [22]. The available scientific literature was used to validate the numerical model.

The main goal of this analysis is to contribute to the performance assessment of new cross-section geometries, with the aim of finding the geometries that enhance the thermal performance of microchannels [23]. To tackle this challenge, a renewed focus on the analysis of the rhombic cross-section is required.

The novelty of this study is the investigation of the effects of viscous heating, which causes an increase in the fluid temperature at the wall, resulting in an increase in the temperature gradient. The role of the temperature gradient can be crucial from a practical point of view. In particular, there are some practical applications in which the temperature gradient must be controlled to avoid the wall temperature reaching the critical value [24]. On the other hand, there are practical applications in which temperature gradients are useful. Among these, Knudsen pumps can be found. In this kind of micropump, the gas flow is induced by the wall temperature gradient [25]. Therefore, the results presented here can be useful for designers and technicians involved in the sizing of microscale heat transfer devices for electronic cooling systems or of Knudsen pumps.

Numerical model

Modeling equations and boundary conditions

The analysis was carried out by considering Newtonian gas with constant properties in fully developed laminar flow-forced convection flowing in a rhombic microchannel (Fig. 1). Under these hypotheses, the momentum and energy balance equations can be written as follows:

$$\mu\left(\frac{\partial^2 u}{\partial^2 x}+\frac{\partial^2 u}{\partial^2 y}\right)=\frac{\partial p}{\partial z} \tag{1}$$

$$\varrho c_p u\frac{\partial T}{\partial z}=\lambda\left(\frac{\partial^2 T}{\partial^2 x}+\frac{\partial^2 T}{\partial^2 y}\right)+\Phi \tag{2}$$

where μ, ρ λ and c_p the fluid viscosity, density, thermal conductivity, and specific heat at constant pressure, respectively; u is the fluid velocity, $\partial p/\partial z$ the pressure gradient along the axial direction; and T is the fluid temperature.

The last term on the right-hand side of Eq. (2) represents the viscous dissipation function that, for incompressible fluids with constant thermophysical properties in the fully developed region, can be expressed as:

$$\Phi=\mu\left[\left(\frac{\partial u}{\partial x}\right)^2+\left(\frac{\partial u}{\partial y}\right)^2\right] \tag{3}$$

By scaling the coordinates by the hydraulic diameter D_h, the fluid velocity by the average velocity W, the pressure gradient by $-\frac{D_h^2}{\mu W}\frac{\partial p}{\partial z}$ and the temperature by $\frac{\lambda T}{qD_h}$, where q represents the wall heat flux, the following dimensionless governing equations can be obtained:

$$\frac{\partial^2 u^*}{\partial^2 x^*}+\frac{\partial^2 u^*}{\partial^2 y^*}=p^* \tag{4}$$

$$\frac{\partial^2 T^*}{\partial^2 x^*}+\frac{\partial^2 T^*}{\partial^2 y^*}=\frac{u^*}{A^*}\left(P^*+Br\int_{A^*}\Phi^* dA^*\right)-Br\Phi^* \tag{5}$$

where A^* is the dimensionless rhombus area ($A^*=A/D_h^2$), P^* is the dimensionless rhombus perimeter ($P^*=P/D_h$), Φ^* the dimensionless viscous dissipation function, and Br is the Brinkman number, which is the ratio of viscous heating to fluid conduction [26]:

$$Br=\frac{\mu W^2}{qD_h} \tag{6}$$

The momentum balance equation in the non-dimensional form was solved by including the slip velocity at the wall because in the present analysis, the slip regime is assumed [1]:

$$u^*-u_w^*=\frac{2-\sigma_v}{\sigma_v}Kn\left(\frac{\partial u^*}{\partial n^*}\right)_w \tag{7}$$

where σ_v represents the momentum accommodation coefficient and Kn is the Knudsen number, which is defined as the ratio of the mean free path over a characteristic length (i.e., the hydraulic diameter in the present analysis).

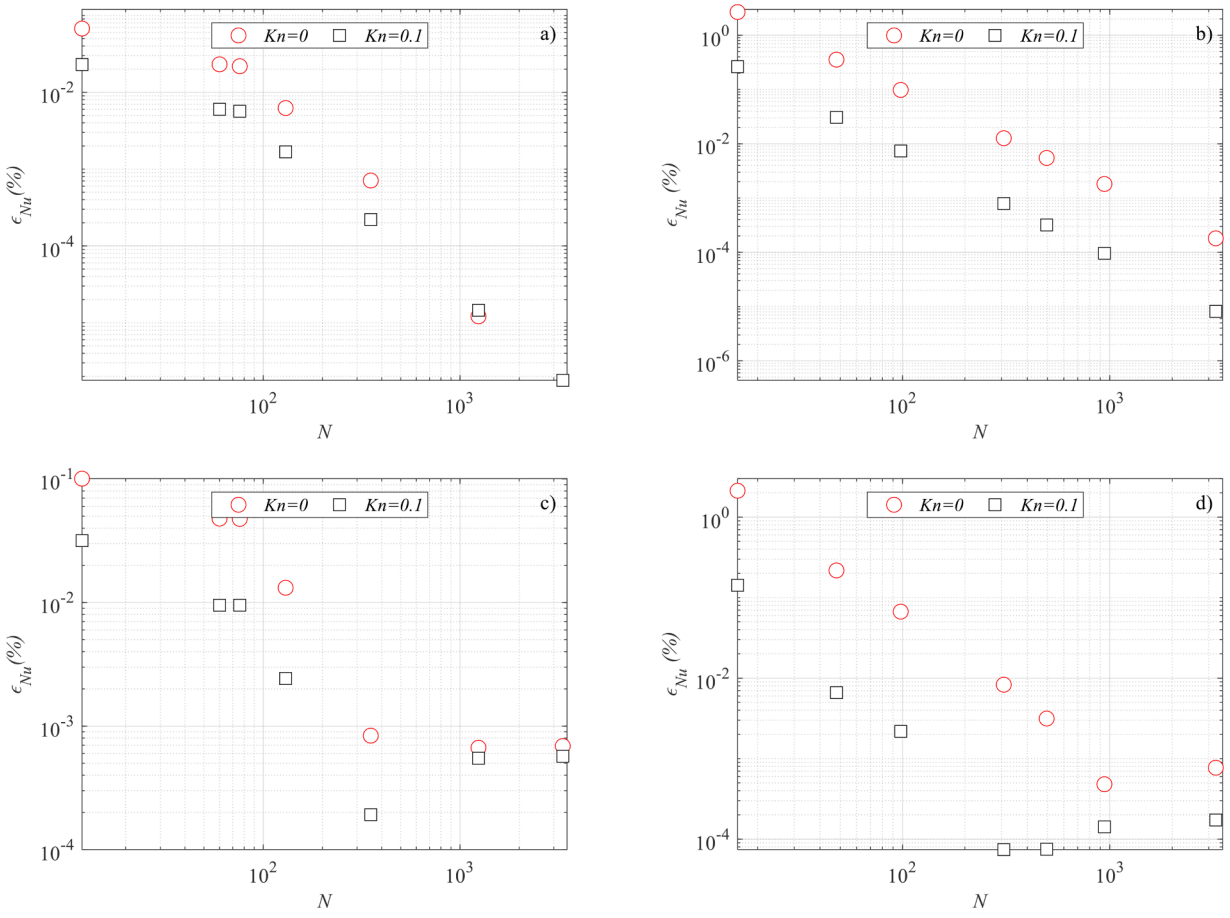

Fig. 2. Relative error on average Nusselt number: (a) $\varphi = 10°$, $Br = 0.01$; (b) $\varphi = 90°$, $Br = 0.01$; (c) $\varphi = 10°$, $Br = 0.1$; and d) $\varphi = 90°$, $Br = 0.1$.

The solution of the thermal energy equation was obtained by assuming that the heat flux at the wall was constant and uniform (the H2 boundary condition):

$$\left(\frac{\partial T^*}{\partial n^*}\right)_w = -1 \tag{8}$$

where n^* is the dimensionless versor normal to the wall.

According to the slip flow model, to evaluate the dimensionless wall temperature, the temperature jump was accounted for as follows:

$$T_w^* = T^* + \frac{2-\sigma_T}{\sigma_T}\frac{2k}{k+1}\frac{Kn}{Pr} \tag{9}$$

where σ_T indicates the thermal accommodation coefficient, k indicates the specific heat ratio, and Pr indicates the Prandtl number. Eq. (9) emphasizes that, with a constant heat flux along the microchannel perimeter, the temperature difference between the solid wall and the gas becomes a constant value, which depends on the Knudsen and Prandtl numbers, the thermal accommodation factor (σ_T) and the gas specific heat ratio (k).

The convective heat transfer coefficient was assessed by evaluating the average Nusselt number:

$$Nu = \frac{hD_h}{\lambda} = \frac{1}{\overline{T_w^*} - T_b^*} \tag{10}$$

where h represents the convective heat transfer coefficient, $\overline{T_w^*}$ and T^*_b are the dimensionless average wall temperature and the dimensionless fluid bulk temperature, respectively.

The dimensionless governing equations were solved by using the partial differential equations interface included in COMSOL®. Second-order elements were used for both fluid velocity and temperature because this scheme works well for low flow velocities [27]. As a convergence criterion, a relative tolerance equal to 1e–06 was imposed.

Mesh independence analysis and model validation

The accuracy of the numerical results was ensured by checking the effects of the number of mesh elements. For the purpose of the present analysis, for each generated mesh, the relative error of the average Nusselt number was assessed:

$$\varepsilon_{Nu} = \left|\frac{Nu_{actual\ mesh} - Nu_{finest\ mesh}}{Nu_{finest\ mesh}}\right| \tag{11}$$

where $Nu_{finestmesh}$ indicates the average Nusselt number evaluated using a reference mesh characterized by an average skewness quality higher than 0.95.

In Fig. 2, the results of the mesh independence analysis are presented for the lowest and highest values of the acute angle and for two values of the Knudsen number: $Kn = 0$ (which corresponds to the no-slip flow) and $Kn = 0.1$ (which corresponds to the upper limit of the slip flow regime). To highlight the sensitivity of the solution to the Brinkman number, two extreme values of Br are considered in Fig. 2 ($Br = 0.01$ and $Br = 0.1$).

It can be observed that a mesh generated with at least 1000 elements guarantees mesh-independent results. Similar conclusions can be drawn by analyzing the results of the mesh independence study for other values of the acute angle.

This indicates that this mesh refinement for each acute angle is sufficiently accurate; consequently, all of the numerical results presented in the next section are obtained at this resolution.

The model accuracy is assessed by means of the available scientific

Table 1
Assessment of model accuracy for $\varphi = 90^\circ$ and $Br = 0.05$ using the numerical data obtained by van Rij et al. [8].

Kn	Nu	Nu [8]	Difference
0	2.647	2.644	0.14 %
0.04	2.644	2.621	0.9 %
0.08	2.429	2.403	1.07 %

Table 2
Assessment of model accuracy for $Kn = 0$ and $Br = 0$ using the numerical values obtained by Shah and London [28].

φ	Nu	Nu [28]	Difference
10	0.068	0.070	−2.41 %
20	0.277	0.279	−0.75 %
30	0.624	0.624	0.06 %
40	1.090	1.090	0.04 %
50	1.630	1.620	0.64 %
60	2.177	2.160	0.79 %
70	2.651	2.640	0.40 %
80	2.973	2.970	0.10 %
90	3.087	3.090	−0.08 %

literature.

More specifically, for $\varphi = 90^\circ$, the numerical results presented by van Rij et al. [8] are assumed to validate the numerical procedure adopted in the present study by considering both rarefaction and viscous dissipation. The maximum disagreement between the present results and the data presented in [8] is about 1 %, as shown in Table 1.

On the other hand, for values of the acute angle lower than 90° the only benchmark that can be found in the literature is represented by the data reported by Shah and London [28] where neither rarefaction nor viscous dissipation are considered. The disagreement between the results presented here and the data presented in [28] is lower than 1 %, with the exception of the rhombus with $\varphi = 10^\circ$, as shown in Table 2.

Results and discussion

The numerical results presented here were obtained by considering Knudsen and Brinkman numbers ranging between 0 and 0.1 and by varying the acute angle of the rhombus in the range of 10° to 90°, keeping the hydraulic diameter constant. Moreover, nitrogen was assumed to be the working gas, and the momentum and thermal accommodation coefficients were assumed to be equal to 1 [1].

In Fig. 3, the contours of the non-dimensional fluid temperature are presented for $\varphi = 60^\circ$ as a function of the Knudsen and Brinkman numbers. As expected, the dimensionless fluid temperature increased with an increasing Brinkman number because of viscous heating. On the

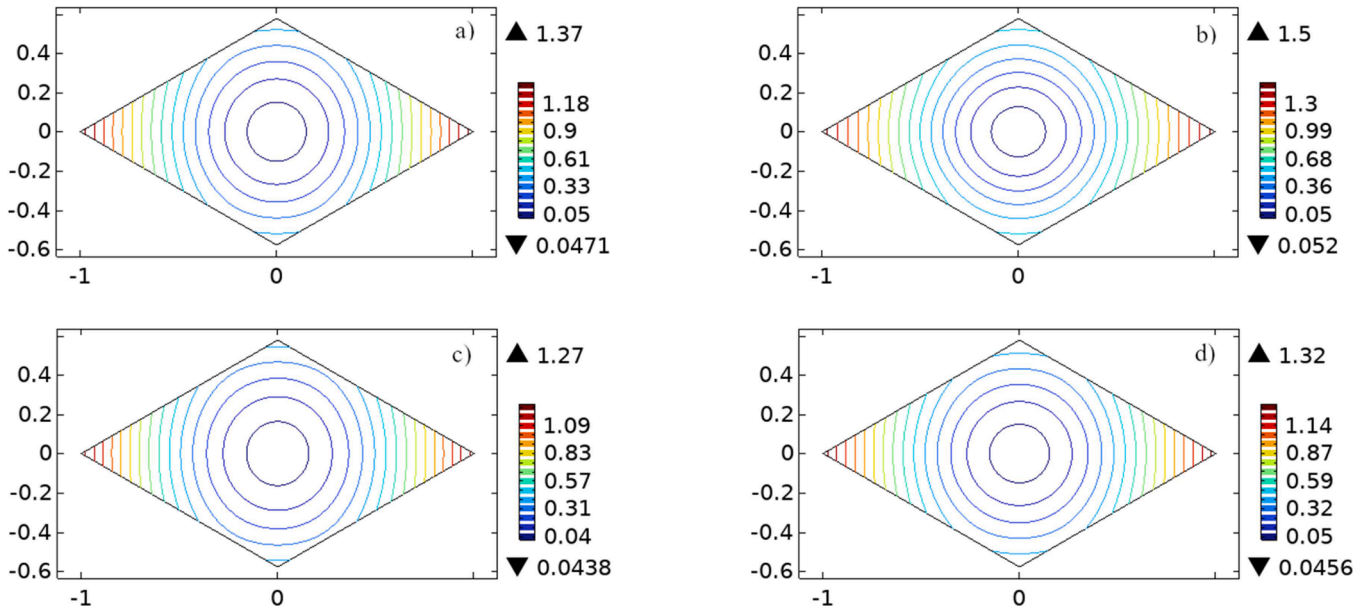

Fig. 3. Dimensionless temperature contours for $\varphi = 60^\circ$: a) $Kn = 0.02$, $Br = 0.01$; b) $Kn = 0.02$, $Br = 0.1$; c) $Kn = 0.1$, $Br = 0.01$; d) $Kn = 0.1$, $Br = 0.1$.

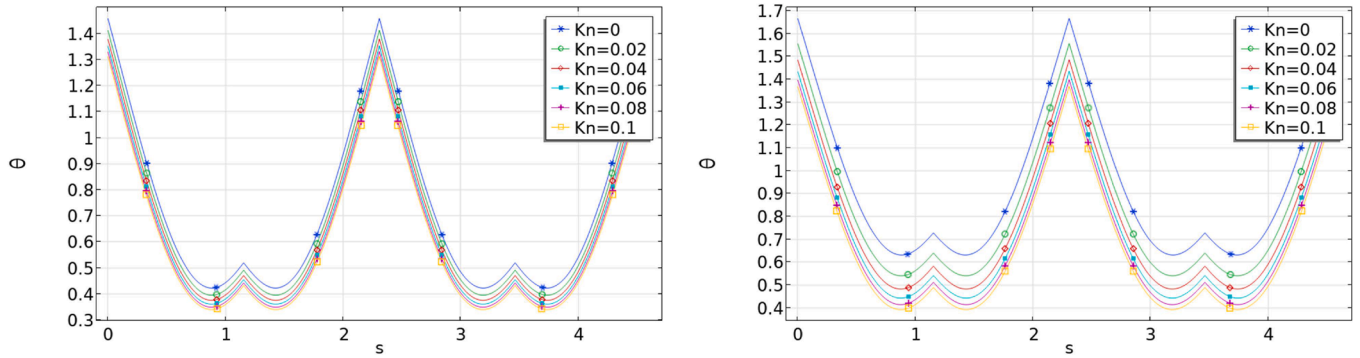

Fig. 4. Viscous dissipation effect on the dimensionless fluid temperature along the perimeter of the rhombus for $\varphi = 60^\circ$: a) $Br = 0.01$; b) $Br = 0.1$.

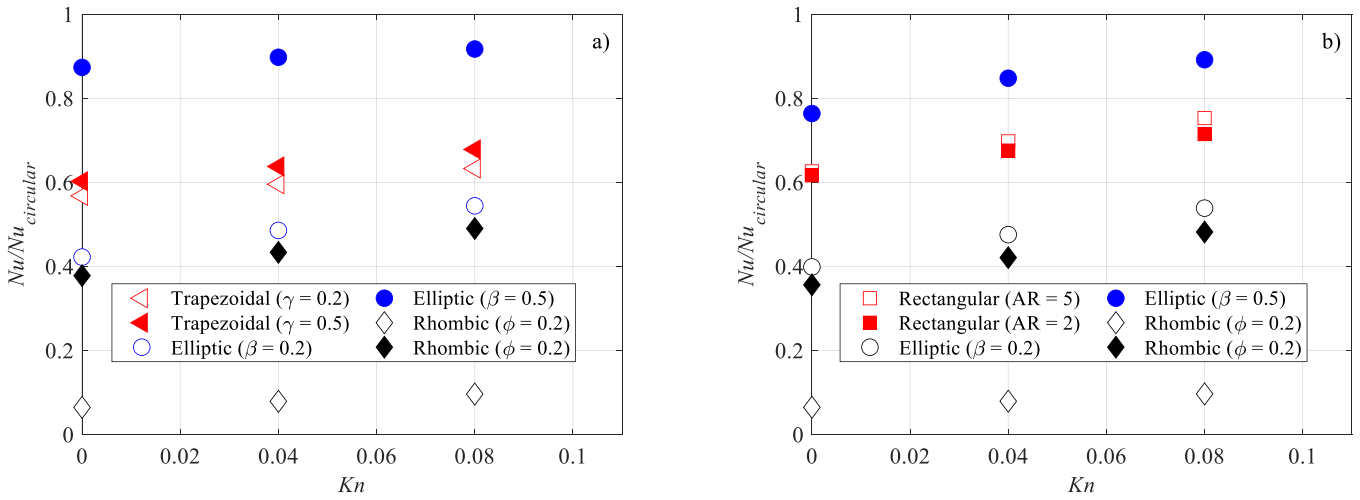

Fig. 5. Comparison between different channel shapes: a) $Br = 0.005$; b) $Br = 0.05$.

other hand, by comparing Fig. 3a) with Fig. 3c) and Fig. 3b) with Fig. 3d), it can be observed that the rarefaction dampens the effect of the viscous forces. This finding can be explained by considering that the velocity gradients decrease with an increasing Knudsen number because of the increase in the slip at the wall.

To highlight the effect of viscous dissipation on the fluid behavior, in Fig. 4 the dimensionless fluid temperature along the perimeter of the rhombus is presented for $\varphi = 60°$. It can be observed that the non-dimensional fluid temperature presents strong variation along the microchannel perimeter; this trend can be explained by remembering

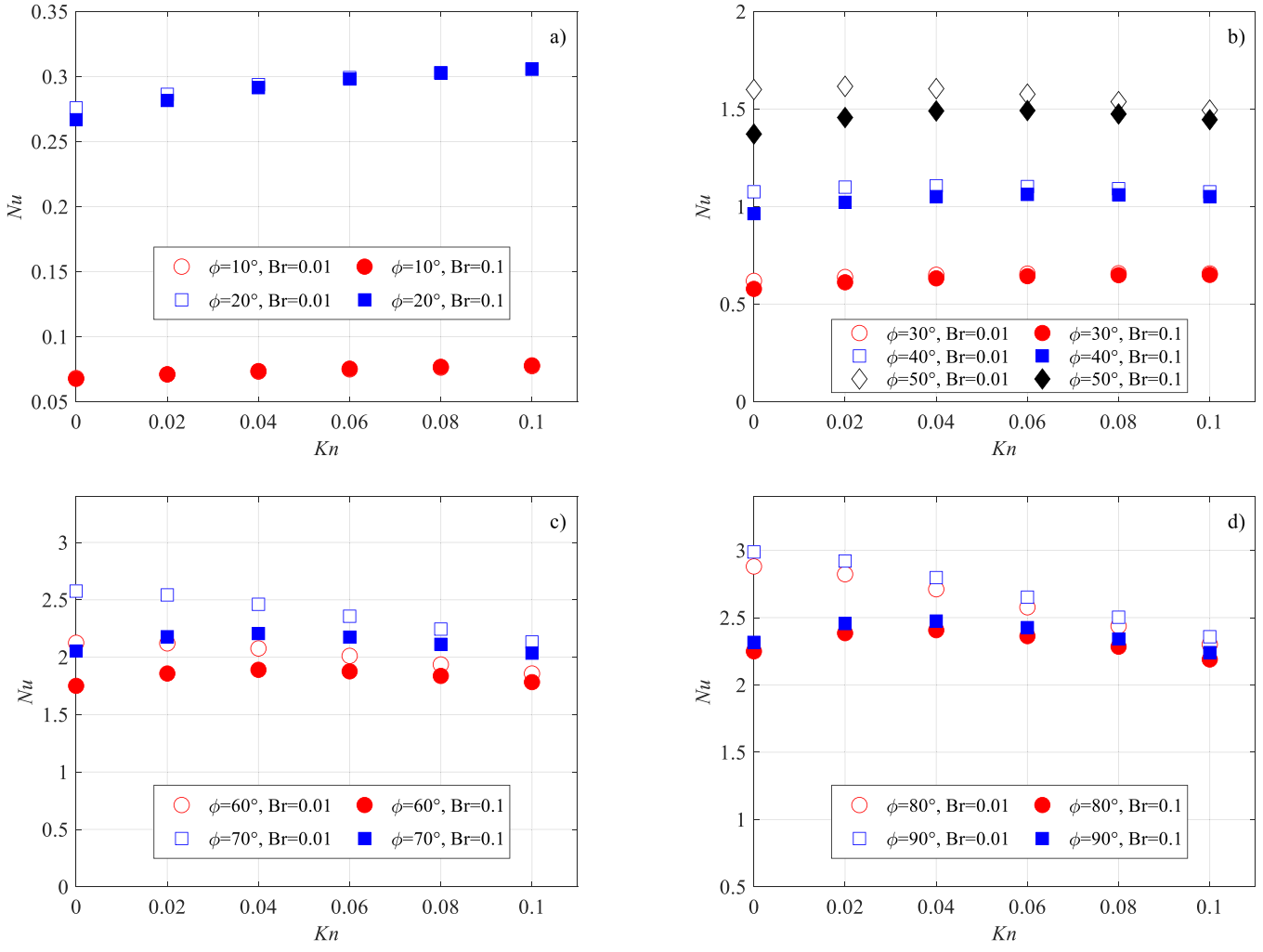

Fig. 6. Viscous dissipation effect on the average Nusselt number: a) $\varphi = 10°$ and $\varphi = 20°$; b) $\varphi = 30°$, $\varphi = 40°$, and $\varphi = 50°$; c) $\varphi = 60°$ and $\varphi = 70°$; d) $\varphi = 80°$ and $\varphi = 90°$.

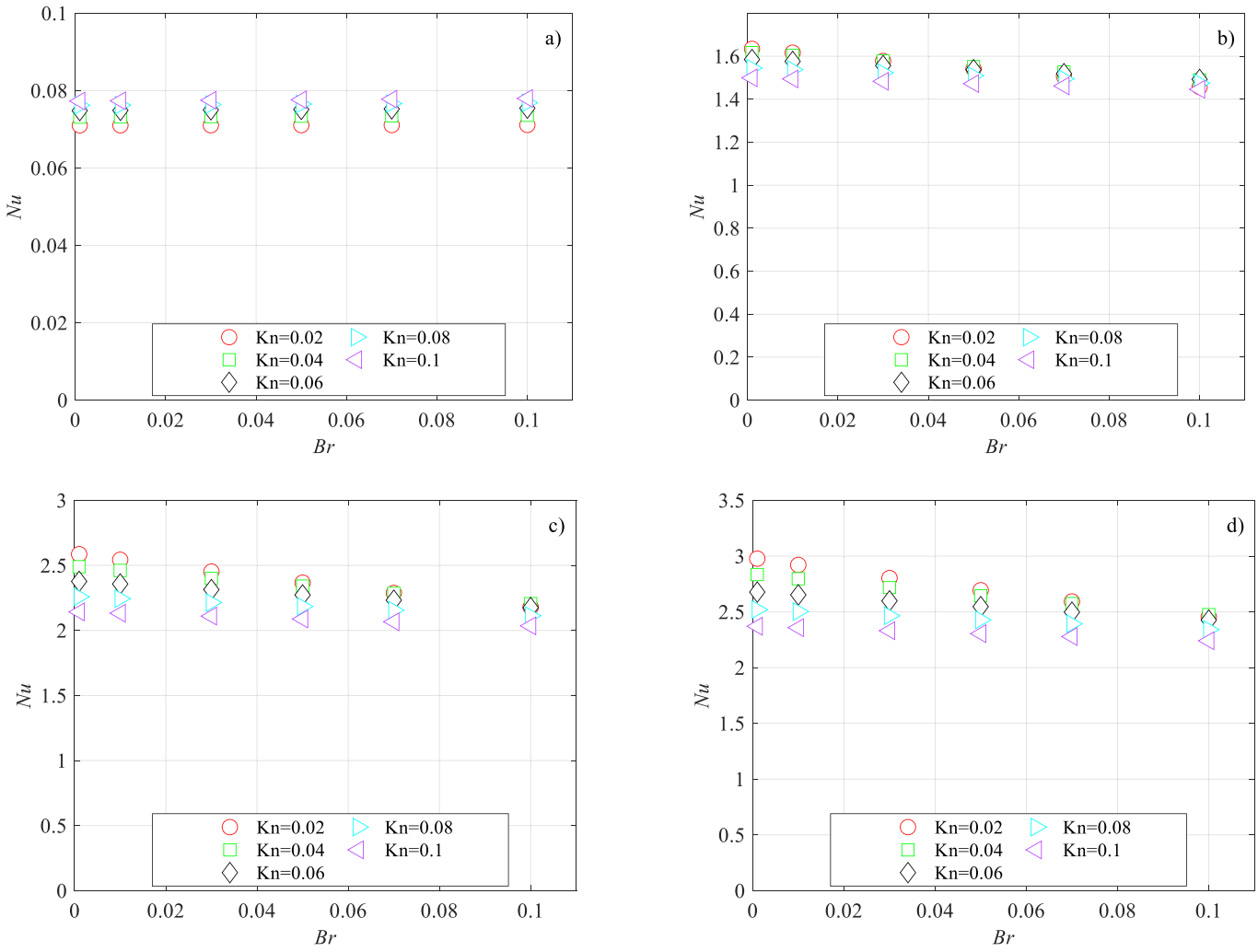

Fig. 7. Average Nusselt number as a function of the Brinkman number: a) $\varphi = 10°$; b) $\varphi = 50°$; c) $\varphi = 70°$; d) $\varphi = 90°$.

that the present analysis was carried out by considering the H2 boundary condition [28]. The fluid temperature variation at the walls results in large thermal stresses in the walls; therefore, it is important to monitor temperature differences.

The maximum values of the fluid temperature trend along the perimeter occurred at acute angles. If the Brinkman number increases, the maximum value of the fluid temperature tends to increase, but if the rarefaction effects are significant, the temperature increase is reduced. This fact confirms that the rarefaction effect tends to contrast with the viscous dissipation effects.

The increase of fluid temperature at the wall caused by viscous dissipation results in an increase in the temperature gradient and consequently in a decrease of the Nusselt number. This effect is marked in Fig. 5, where the trends of *Nu* are presented for several combinations of the main parameters affecting fluid behavior. In particular, the Nusselt number decreases as the Brinkman number increases for each value of the acute angle of the rhombus and for each value of the Knudsen number. This result is in agreement with the observations of van Rij et al. [8], Kuddusi [9], and Vocale et al. [10], who investigated the role of viscous dissipation in rectangular, trapezoidal, and elliptical microchannels, respectively. To highlight the influence of channel shape, a comparison between the performance of different microchannels in terms of the average Nusselt number was performed. In particular, the ratio between the average Nusselt number for other geometries and the Nusselt number for circular microchannels was evaluated (i.e., because the circular cross-section guarantees the best thermal performance, it was chosen as reference).

In Fig. 5, the comparison between the different cross-section geometries (i.e. rectangular [8], trapezoidal [9], elliptic [10] and rhombic) is presented for some referenced cases. It can be observed that because of the presence of corners, the thermal performance of both rectangular and rhombic cross-sections are lower than elliptic ones, with the exception of the elliptic microchannels characterized by low values of the aspect ratio that present performance similar to the rhombic cross-section. It can also be observed that the Nusselt number ratio increases with increasing Knudsen number; this effect can be explained by considering that as the rarefaction degree increases, the slip velocity at the wall increases. Therefore, the influence of the corners becomes less pronounced.

With the regards to the rhombic microchannels, it was also observed that the reduction in the average Nusselt number became less pronounced as the Knudsen number increased. This effect was due to the reduction of the velocity gradients with an increasing Knudsen number linked to the increase in the slip at the wall. On the other hand, the reduction in the average Nusselt number becomes more marked as the value of the acute angle increases. This effect is due to the increase of the Poiseuille number and the dimensionless area with decreasing acute angle of the rhombus [20]. Morini et al. [29] demonstrated that the ratio of the temperature gradient caused by wall heat flux to the temperature gradient caused by viscous dissipation is proportional to the Brinkman number, the dimensionless area, and the Poiseuille number.

However, the trend of *Nu* may vary significantly depending on the

Table 3
Rate of change in the average Nusselt number.

φ	Minimum reduction in *Nu*	Maximum reduction in *Nu*
10	0.9 %	1.0 %
20	0.1 %	3.6 %
30	1.2 %	7.4 %
40	2.5 %	11.6 %
50	3.6 %	15.8 %
60	4.5 %	19.6 %
70	5.1 %	22.5 %
80	5.4 %	24.3 %
90	5.5 %	25.0 %

value of the acute angle of the rhombus and the Brinkman number, as shown in Fig. 6. In particular, for $\varphi = 10^\circ$ and $\varphi = 20^\circ$ (Fig. 6a), the average Nusselt number increases with an increasing Knudsen number for both values of the Brinkman number. Moreover, pure heat conduction is more effective than convective heat transfer because the average Nusselt number is lower than 1. Similar trends were also observed in elliptical microchannels [10].

On the other hand, for $\varphi = 30^\circ$, different trends of the average Nusselt number were observed; in particular, the variation of the *Nu* is non-monotonic with the presence of a peak for $Br = 0.01$, while *Nu* increases with increasing Knudsen number for $Br = 0.1$. Fig. 6b shows a non-monotonic variation in the average Nusselt number as a function of the Knudsen number for $\varphi = 40^\circ$ and $\varphi = 50^\circ$ for both Brinkman numbers.

Figs. 6c and d show a decreasing trend in the average Nusselt number with an increasing Knudsen number for φ ranging between 60° and 90° only for $Br = 0.01$, while for $Br = 0.1$, the presence of a peak in the *Nu* trends can be observed.

By analyzing the data reported in Fig. 6 it is possible to observe that the influence of the viscous dissipation on the average Nusselt number increases with increasing acute angle. This effect is more evident in Fig. 7, where the trend of *Nu* as a function of the Brinkman number is presented for four values of the acute angle. In particular, it can be observed that Nu is significantly affected by the Brinkman number for acute angles higher than 50°.

With the aim to help the designers, the maximum and minimum reduction in the average Nusselt number is reported in Table 3 for each value of the acute angle considered in this study. As discussed previously, the maximum reduction in the Nusselt number is observed for continuum flow (i.e., $Kn = 0$).

Conclusion

In this work, a numerical investigation of the viscous heating effect on the thermal performance of laminar gaseous flows in a slip regime through rhombus microchannels is presented. The solution of the dimensionless momentum and energy equations have been obtained by using the PDI interface included in Comsol®, including the slip velocity and the temperature jump at the wall. The model validation was carried out using the available scientific literature.

The main results of the numerical investigation presented here can be summarized as follows:

- Viscous dissipation effects lead to a decrease in the average Nusselt number; the reduction depends on the values of the acute angle of the rhombus and the Knudsen number.
- For rhombic microchannels characterized by low values of the acute angle ($\varphi \leq 30^\circ$) the viscous dissipation is able to reduce the value of the average Nusselt number up to 8 % with respect to the case of negligible viscous dissipation ($Br = 0$), while for squared microchannels ($\varphi = 90^\circ$), the average Nusselt number may be reduced up to 25 %.
- The maximum decrease in the average Nusselt number occurs for continuum flow because rarefaction effects tend to reduce the value of the velocity gradients and, as a consequence, dampen the effect linked to the viscous dissipation of the convective heat transfer.

It is possible to conclude that in the presence of rarefaction effects in microchannels, the role played by viscous dissipation on the convective heat transfer is strongly reduced when compared with the case of continuum flow.

CRediT authorship contribution statement

Pamela Vocale: Writing – original draft, Validation, Methodology, Investigation, Data curation, Conceptualization. **Gian Luca Morini:** Writing – review & editing, Supervision, Methodology.

Declaration of competing interest

The authors declare that they have no known competing financial interests or personal relationships that could have appeared to influence the work reported in this paper.

Data availability

Data will be made available on request.

References

[1] Karniadakis G., Beskok A., Aluru N. 2005. Microflows and nanoflows - fundamentals and simulation.
[2] G. Tunc, Y. Bayazitoglu, Heat transfer in microtubes with viscous dissipation, Int. J. Heat Mass Transf. 44 (2001) 2395–2403, https://doi.org/10.1016/S0017-9310(00)00298-2.
[3] B. Cetin, A.G. Yazicioglu, S. Kakac, Fluid flow in microtubes with axial conduction including rarefaction and viscous dissipation, Int. Commun. Heat Mass Transf. 35 (2008) 535–544, https://doi.org/10.1016/j.icheatmasstransfer.2008.01.003.
[4] B. Cetin, A.G. Yazicioglu, S. Kakac, Slip-flow heat transfer in microtubes with axial conduction and viscous dissipation – an extended Graetz problem, Int. J. Therm. Sci. 48 (2009) 1673–1678, https://doi.org/10.1016/j.ijthermalsci.2009.02.002.
[5] H. Bahrami, T.L. Bergman, A. Faghri, Forced convective heat transfer in a microtube including rarefaction, viscous dissipation and axial conduction effects, Int. J. Heat Mass Transf. 55 (2012) 6655–6675, https://doi.org/10.1016/j.ijheatmasstransfer.2012.06.075.
[6] H.L. Liu, X.D. Shao, J.Y. Jia, Effects of axial heat conduction and viscous dissipation on heat transfer in circular microchannels, Int. J. Therm. Sci. 66 (2013) 34–41, https://doi.org/10.1016/j.ijthermalsci.2012.11.007.
[7] S. Şen, S. Darici, Transient conjugate heat transfer in a circular microchannel involving rarefaction, viscous dissipation and axial conduction effects, Appl. Therm. Eng. 111 (2017) 855–862, https://doi.org/10.1016/j.applthermaleng.2016.10.005.
[8] J. van Rij, T. Ameel, T. Harman, The effect of viscous dissipation and rarefaction on rectangular microchannel convective heat transfer, Int. J. Therm. Sci. 48 (2009) 271–281, https://doi.org/10.1016/j.ijthermalsci.2008.07.010.
[9] L. Kuddusi, First and second law analysis of fully developed gaseous slip flow in trapezoidal silicon microchannels considering viscous dissipation effect, Int. J. Heat Mass Transf. 54 (2011) 52–64, https://doi.org/10.1016/j.ijheatmasstransfer.2010.09.064.
[10] P. Vocale, G. Puccetti, G.L. Morini, M. Spiga, Numerical investigation of viscous dissipation in elliptic microducts, J. Physics: Conf. Ser. 547 (2014) 012023, https://doi.org/10.1088/1742-6596/547/1/012023.
[11] D.-K. Lee, J.Y. Kwon, Y.H. Cho, Fabrication of microfluidic channels with various cross-sectional shapes using anisotropic etching of Si and self-alignment, Appl. Phys. A 125 (2019), https://doi.org/10.1007/s00339-019-2600-2. Article number: 291.
[12] S.K. Saha, A. Agrawal, Y. Soni, Heat transfer characterization of rhombic microchannel for H1 and H2 boundary conditions, Int. J. Therm. Sci. 111 (2017) 223–233, https://doi.org/10.1016/j.ijthermalsci.2016.09.003.
[13] M. Bahrami, Y.M. Michael, C.J. Richard, A novel solution for pressure drop in singly connected microchannels of arbitrary cross-section, Int. J. Heat Mass Transf. 50 (2007) 2492–2502, https://doi.org/10.1016/j.ijheatmasstransfer.2006.12.019.
[14] A. Tamayol, M. Bahrami, Laminar flow in microchannels with noncircular cross section, ASME J. Fluids Eng. 132 (2010) 111201, https://doi.org/10.1115/1.4001973.
[15] S. Shahsavari, A. Tamayol, E. Kjeang, M. Bahrami, Convective heat transfer in microchannels of noncircular cross sections: an analytical approach, ASME J. Heat Transf. 134 (2012) 91701, https://doi.org/10.1115/1.4006207.

[16] A. Tamayol, K. Hooman, Slip-flow in microchannels of non-circular cross sections, ASME J. Fluids Eng. 133 (2011) 091202, https://doi.org/10.1115/1.4004591.
[17] M. Baghani, A. Sadeghi, Gaseous slip flow forced convection in microducts of arbitrary but constant cross section, Nanoscale Microscale Thermophys. Eng. 18 (2014) 354–372, https://doi.org/10.1080/15567265.2014.948232.
[18] S. Mukherjee, P. Biswal, Chakraborty, et al., Effects of viscous dissipation during forced convection of power-law fluids in microchannels, Int. Commun. Heat Mass Transf. 89 (2017) 83–90, https://doi.org/10.1016/j.icheatmasstransfer.2017.09.018.
[19] A.K.W. Loh, G.M. Chen, B.K. Lim, Viscous dissipation effect on forced convective transport of nanofluids in an asymmetrically heated parallel-plate microchannel, Case Stud. Therm. Eng. 35 (2022) 102056, https://doi.org/10.1016/j.csite.2022.102056.
[20] M. Shams, M. Shojaeian, C. Aghanajafi, S.A.R. Dibaji, Numerical simulation of slip flow through rhombus microchannels, Int. Commun. Heat Mass Transf. 36 (2009) 1075–1081, https://doi.org/10.1016/j.icheatmasstransfer.2009.07.010.
[21] P. Vocale, G.L. Morini, Thermal characterisation of rarefied flows in rhombic microchannels, Micromachines (Basel) 14 (2023) 2222, https://doi.org/10.3390/mi14122222.
[22] S Colin, Rarefaction and compressibility effects on steady and transient gas flows in microchannels, Microfluid Nanofluid 1 (2005) 268–279, https://doi.org/10.1007/s10404-004-0002-y.
[23] K. Lu, C. Wang, C. Wang, et al., Topological structures for microchannel heat sink applications - a review, Manuf. Rev. (Les. Ulis) 10 (2023) 480–490, https://doi.org/10.1051/mfreview/2022035.
[24] K. Rezk, M.A. Abdelrahman, A.A.A. Attia, M. Emam, Thermal control of temperature-sensitive electronic components using a vapor chamber integrated with a straight fins heat sink: an experimental investigation, Appl. Therm. Eng. 217 (2022) 119147, https://doi.org/10.1016/j.applthermaleng.2022.119147.
[25] X. Wang, T. Su, W. Zhang, Z. Zhang, et al., Knudsen pumps: a review, Microsyst. Nanoeng. 6 (2020) 26, https://doi.org/10.1038/s41378-020-0135-5.
[26] C.P. Tso, S.P. Mahulikar, The use of the Brinkman number for single phase forced convective heat transfer in microchannels, Int. J. Heat Mass Transf. 41 (1998) 1759–1769, https://doi.org/10.1016/S0017-9310(97)00232-9.
[27] COMSOL Multiphysics. 2023. Reference manual.
[28] Shah R.K., London A.L. 1978. Laminar flow forced convection in ducts.
[29] G.L. Morini, M. Spiga, The Role of the Viscous Dissipation in Heated Microchannels, ASME J. Heat Transf. 129 (2007) 308–318, https://doi.org/10.1115/1.2430725.